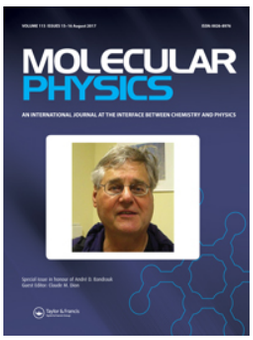

Taylor & Francis
Taylor & Francis Group

Molecular Physics

An International Journal at the Interface Between Chemistry and Physics

ISSN: 0026-8976 (Print) 1362-3028 (Online) Journal homepage: http://www.tandfonline.com/loi/tmph20

Signatures of transient electron localisation in high-order harmonic generation

M. R. Miller, A. Jaroń-Becker & A. Becker

To cite this article: M. R. Miller, A. Jaroń-Becker & A. Becker (2017) Signatures of transient electron localisation in high-order harmonic generation, Molecular Physics, 115:15-16, 1758-1767, DOI: 10.1080/00268976.2016.1262554

To link to this article: https://doi.org/10.1080/00268976.2016.1262554

Published online: 27 Dec 2016.

MOLECULAR PHYSICS, 2017
VOL. 115, NOS. 15–16, 1758–1767
http://dx.doi.org/10.1080/00268976.2016.1262554

Taylor & Francis
Taylor & Francis Group

BANDRAUK

Signatures of transient electron localisation in high-order harmonic generation

M. R. Miller, A. Jaroń-Becker and A. Becker

JILA and Department of Physics, University of Colorado, Boulder, CO, USA

ABSTRACT

We identify and explain signatures of ongoing single-electron nonadiabatic dynamics in the high-order harmonic generation (HHG) spectrum of H_2^+. We establish the necessary laser parameter criteria for the modulation of the highest energy section of the HHG spectrum by suppressed ionisation due to transient electron localisation. This minimum is also shown to enable the emergence of an unusually complex interference structure at the highest energies of the spectrum caused by the breaking of inversion symmetry during sequential recombination events of the electron wavepacket. By inspecting the time-domain structure of the emitted radiation, we identify the role of transient electron localisation in modulating the amplitudes of individual peaks within the attosecond pulse train. Finally, an analysis of the phase mismatch accumulated within this highly structured region of HHG is performed, showing qualitative differences in coherence lengths present in different regions of the spectrum.

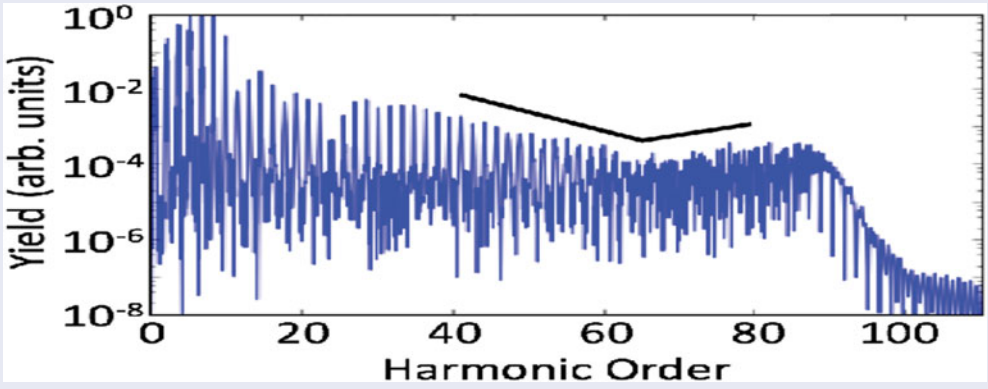

ARTICLE HISTORY
Received 2 June 2016
Accepted 28 October 2016

KEYWORDS
High-order harmonic generation; strong-field effects; nonadiabatic electron dynamics

1. Introduction

Nonadiabatic electron dynamics induced by interactions with strong laser fields occur beyond standard quasi-static descriptions of electron response. In addition, they possess the capacity to modify many common signals of strong-field physics. As higher laser intensities and longer wavelengths become increasingly accessible to experimental and theoretical studies, nonadiabatic electron dynamics are more likely to result. These dynamics present an avenue for the observation of and control over electron motion through several strong-field -induced mechanisms [1]. Investigations of such phenomena have implicated nonadiabatic electronic behaviour as a critical determinant of fragmentation patterns [2–4], photoelectron distributions [5,6], ionisation rates [7–9], and high-order harmonic generation (HHG) spectra [10,11].

Among these signals, HHG in particular presents a method of uncovering both ionisation and dynamical behaviour of the electron in response to the laser field. According to the conventional three-step description of this effect, the total signal of HHG is shaped by the ionisation of the electron into the continuum, the subsequent propagation of the electron in the electric field, and the radiation-emitting recombination of the electron wavepacket with the residual parent ion [12,13]. Each step of this process encodes information regarding the behaviour of the electron, reflected in both the amplitude and phase of the harmonics emitted [14,15]. From a practical perspective, modification of the HHG signal

CONTACT A. Becker andreas.becker@colorado.edu
We dedicate this article to Prof. Andre D. Bandrauk on the occasion of his 75th birthday.

additionally enables control over the resultant attosecond pulses (1 as $= 10^{-18}$ s), offering a means for shaping or modifying the spectral content of pulses used for further experimentation.

In this paper, we analyse a particular case of nonadiabatic electron dynamics which manifests through the transient localisation of the electron upon alternating sides of the hydrogen molecular ion (H_2^+) [16,17]. As a single-active electron system, H_2^+ serves as an ideal theoretical model to distinguish signatures of single-electron nonadiabaticity from multielectron effects. Additionally, nonadiabatic dynamics in H_2^+ are known to occur at extended internuclear distances, affecting the time-dependent ionisation rate and modifying the internal electron distribution through an intramolecular dynamic [1]. Transient localisation has previously been implicated in the creation of a minimum in the HHG spectrum when driven with a laser possessing suitable wavelength and intensity [10]. Here, we first further explore the system conditions resulting in the modulation of the spectral amplitude of HHG. In addition, we consider additional signatures of transient electron localisation in the HHG signal. To this end, we characterise and explain a specific interference structure, exploring the transition from conventional odd harmonic generation to a more complex high-energy structure. Furthermore, we analyse the time-domain structure of the emitted pulse train. Finally, we explore the relationship between the phase encoded within the harmonics and the capacity for different energies to phase-match sufficiently to enable experimental detection. We end the manuscript with concluding remarks.

2. Methods

Calculations were performed by solving the time-dependent Schrödinger equation (TDSE) for electron motion in three dimensions using a standard Crank–Nicholson method. A fixed-nuclei model of H_2^+ was exposed to a linearly polarised laser field, assuming alignment of the internuclear axis with the laser polarisation direction. The Hamiltonian for this system ($e = \hbar = m = 1$) is given by

$$H(t) = -\frac{1}{2}\left(\frac{1}{\rho}\frac{\partial}{\partial\rho}\rho\frac{\partial}{\partial\rho} + \frac{\partial^2}{\partial z^2}\right) - \frac{1}{\sqrt{\rho^2 + (z+\frac{R_0}{2})^2}} - \frac{1}{\sqrt{\rho^2 + (z-\frac{R_0}{2})^2}} + zE(t), \quad (1)$$

where R_0 is the internuclear distance of the molecular ion, and $E(t) = E_0\cos(\omega t)\sin^2(\pi t/N\tau)$ is the electric field. In this study, the value of $R_0 = 7$ a.u. The spatial grid possessed $\Delta z = 0.1$ a.u. and $\Delta\rho = 0.0375$ a.u. with a time step $\Delta t = 0.01$ a.u. In total, the numerical grid occupied 400 points (15 a.u.) in the ρ direction and was adjusted in the z direction to exceed four times the electron quiver radius for each set of laser parameters considered in the present study.

The initial ground state of the wavefunction was calculated using imaginary time propagation, resulting in initial energies of -0.505 a.u. and -0.496 a.u. for the $|g\rangle$ and $|u\rangle$ states, respectively. The ground state was propagated in time under the influence of the laser field, and the time-dependent wavefunction was obtained to compute HHG spectra as the Fourier transform of the dipole acceleration. Time-resolved frequency information was obtained by computing the wavelet analysis of the dipole acceleration $d_{a_z}(t)$ as

$$C(t_0,\omega) = \frac{1}{\sqrt{2\pi}}\int_0^T d_{a_z}(t)W\left(\frac{\omega(t-t_0)}{2\pi}\right)dt, \quad (2)$$

where $W(x) = \frac{1}{\sqrt{\pi}}\exp(2\pi ix)\exp(-x^2)$ is the complex Morlet wavelet. This was used to examine the amplitude of radiation emerging from isolated recombination events.

In the context of studying single-electron nonadiabatic electron dynamics induced by intense laser fields, H_2^+ is a useful model due to the simplicity of the system. Symmetric molecular ions such as H_2^+ possess pairs of charge-resonant states which, throughout a regime of critical internuclear distances, become nearly degenerate and couple strongly to electromagnetic fields. In the case of H_2^+, the $|g\rangle$ and $|u\rangle$ states play a dominant role in the laser-induced ionisation of the system as it dissociates, amplifying the ionisation rate by one to three orders of magnitude in models including both electronic and nuclear motion [18] and inducing nonadiabatic electron dynamics. The theoretical simplicity of the charge-resonant states has permitted substantial analytical work toward resolving the time-dependent behaviour of an electron undergoing nonadiabatic dynamics in the H_2^+ system, including the transient localisation of the electron on the counterintuitive side of the molecule at the peak of each laser field half-cycle. These instants of localisation were predicted to occur at times t_{loc} satisfying [16,17,19]

$$A(t_{loc}) = \frac{m\pi}{2\langle g|z|u\rangle} \qquad \text{with } m = 0, \pm1, \pm2, \ldots, \quad (3)$$

where $A(t) = A_0\sin(\omega t + \phi)$ approximates the vector potential near the peak of the electric field pulse, we set the phase $\phi = 0$, and d_{gu} represents the dipole transition matrix element between the $|g\rangle$ and $|u\rangle$ states.

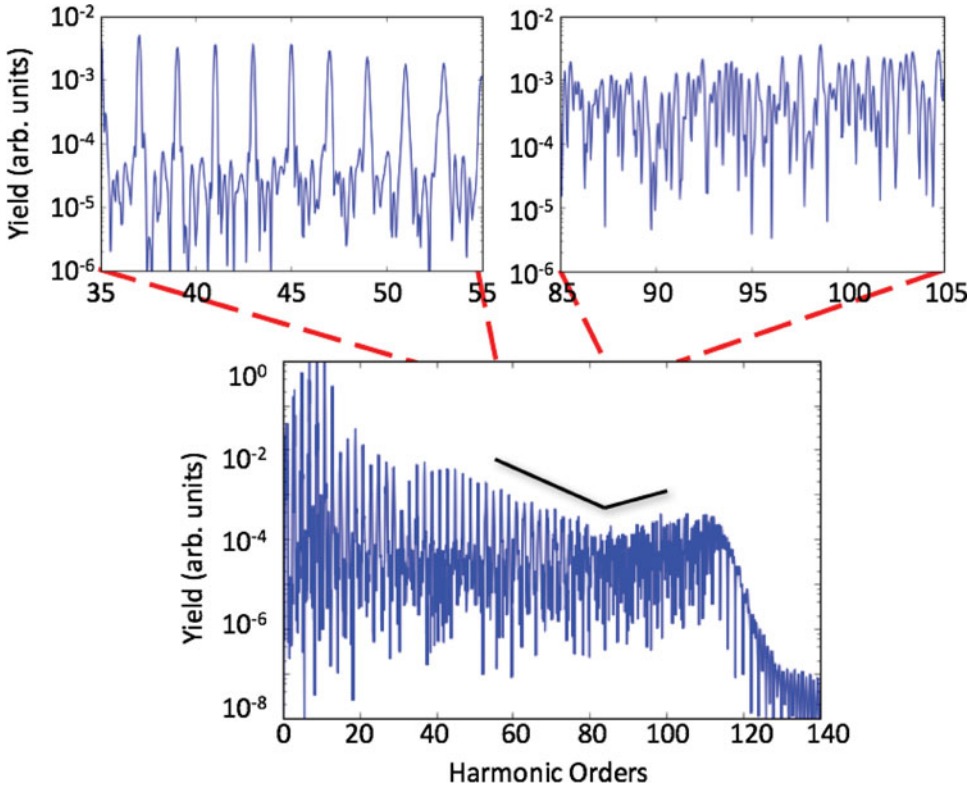

Figure 1. (Colour online) Transient localisation imprints two features upon the radiated HHG spectrum: a minimum in the harmonic spectrum, and non-odd harmonic generation. In the lower panel, black lines indicate the structure of the minimum in the spectrum, which presents as a modulation of yield into an interval of energies. The two upper panels contrast the interference structure of the spectrum, demonstrating the progression of conventional odd harmonic generation (left) to non-odd harmonic generation (right). Results are presented for a 20 -cycle full width, 1.8-m driving laser with intensity 6×10^{13} W cm^{-2}.

The nonadiabatic dynamics is closely related to the evolving phase difference between the electron wavefunction centred upon each of the two protons in H_2^+ [17,19]

$$\alpha(t) = \arg\left[\Psi\left(\frac{\Delta\rho}{2}, \frac{R_0}{2}; t\right)\right] - \arg\left[\Psi\left(\frac{\Delta\rho}{2}, -\frac{R_0}{2}; t\right)\right], \tag{4}$$

At moments when the electron is most localised upon the counter-intuitive side of the molecule, $\alpha = 0$ [10,16].

3. Signatures of nonadiabatic electron dynamics

The HHG spectrum in Figure 1, obtained at a central wavelength of 1.8 m at peak intensity 6×10^{13} W cm^{-2}, shows two signatures that we attribute to nonadiabatic electron dynamics and transient localisation of the electron: a minimum at about harmonic order 65 and the appearance of non-odd harmonics in the spectrum. More specifically, as demonstrated in the upper panels, the variation occurs in the part of the spectrum beyond the minimum. In this section, we will analyse and discuss both these features, as well as the effects of transient electron localisation on the attosecond pulse train.

3.1. Transient electron localisation and suppression of HHG

The connection between the formation of a minimum in HHG and the laser-driven transient localisation of the electron wavepacket was established in [10]. In this study, ionisation suppression was identified as the mechanism which modulated the amplitude of the harmonic generation at related energy values. Ionisation is suppressed due to the ongoing transient localisation of the electron upon the downhill electronic well, from which ionisation is no longer favoured. However, as we will now show, observing transient localisation is not a sufficient criterion for a modulation of the HHG spectrum. We will discuss this effect first qualitatively, using HHG signals obtained at different wavelengths (see Figure 2), and then analyse it further, based on a wavelet analysis (see Figure 3).

According to Equation (3), localisation behaviour in fixed-nucleus extended H_2^+ is highly sensitive both to

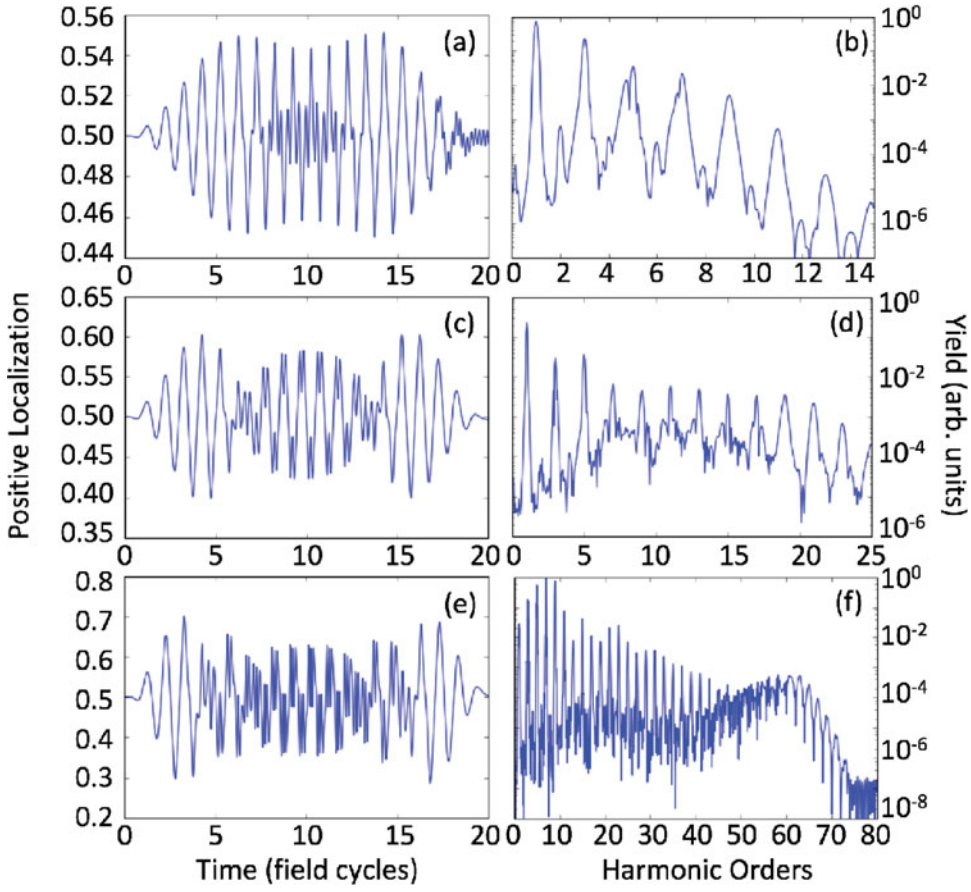

Figure 2. (Colour online) Increasing the wavelength of the driving field enhances the nonadiabatic behaviour displayed by the oscillating electron, which ultimately modulates the high-energy plateau of the harmonic spectrum. In all cases, a 20-cycle, 6×10^{13} W cm^{-2} laser field is used. (a) Driving at 400 nm results in largely adiabatic behaviour except at the peak of the laser field, when the onset of transient localisation is observed. The corresponding harmonic spectrum (b) does not appear modulated and presents the conventional generation of odd harmonics. (c) Increasing the driving wavelength to 800 nm results in clear signatures of transient localisation occurring twice per half-field cycle throughout the peak of the pulse. The HHG spectrum (d) driven by this field continues to show no evidence of nonadiabatic behaviour. Further increase of the driving wavelength to 1.4 m (e) exhibits a transition from two to three localisations per half-field cycle as the field strength increases. This nonadiabatic response can be identified in the HHG spectrum (f) through a modulation of the HHG plateau, achieving a minimum at 47 harmonic orders. In addition, a complex interference structure appears at energies exceeding the 47th harmonic order.

intensity and to wavelength of the laser field [16]. We therefore begin with a qualitative study illustrating the relation between transient electron localisation and HHG suppression by changing the wavelength of the driving laser. In Figure 2(a,c,e), the probability for electron occupation of the $z > 0$ section of the spatial grid is demonstrated throughout all field cycles. In Figure 2(b,df), the corresponding HHG spectrum is shown. In each case, the electron responds adiabatically to the laser field throughout the first several cycles of laser exposure. At the shortest driving wavelength shown, in Figure 2(a), the electron behaviour remains relatively adiabatic throughout the central cycles of the laser field as well. The HHG spectrum produced by this wavelength (Figure 2(b)) consequently shows conventional spectral features: odd harmonic peaks are well isolated, and the efficiency of harmonic production throughout the plateau energies remains constant.

With increasing wavelength, the adiabatic behaviour initially observed is seen to transition rapidly to a nonadiabatic dynamic. The nonadiabaticity of the electron motion can be identified by examining the electron localisation in Figure 2(c), and noting the qualitative departure of the distribution from the shape of the electric field. Between 7th and 13th field cycle, the electron is observed to travel against the gradient of the laser field once per half-field cycle. This dynamic results in the double-peak feature observed in the positive localisation throughout the nonadiabatic interval. Despite this evidence of nonadiabatic intramolecular motion, the HHG spectrum generated by these laser parameters continues to demonstrate conventional features. Localisation of the electron

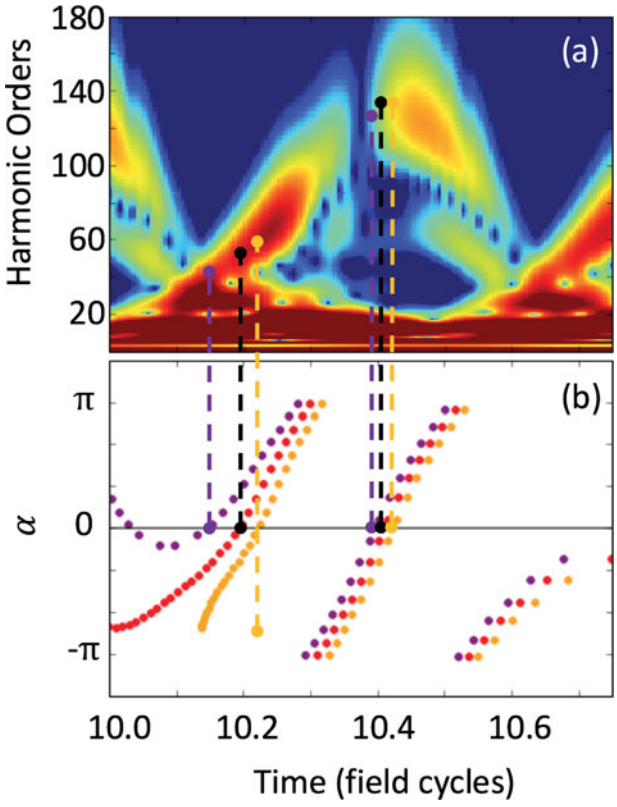

Figure 3. Classical approximation of the returning electron enables the connection of ionisation suppression during ionisation to minima in harmonic generation for HHG driven by 20-cycle, 1.4 m, 1.8 × 10^{14} W cm^{-2} light. In panel (a), the time-frequency analysis of radiation emission during a central cycle of the laser field used in Figure 1 reveals two instants of suppressed emission. In (b), the predictions of classical analyses considering different initial and final position criteria for the propagating point electron are shown as an estimation of the uncertainty involved in this calculation. The classical analysis enables the extraction of electron dynamics at the time of ionisation for each recombination time indicated along the *x*-axis. These associated ionisation dynamics are the quantity shown in (b).

wavepacket twice per field cycle positions this moment of suppressed ionisation near the maximum of the field and, hence, at an imperceptible time instant to HHG. Consequently, there is no evidence of the transient localisation via a minimum in the HHG spectrum (c.f. Figure 2(d)).

However, as the nonadiabatic character of the electron dynamic is augmented by selecting laser parameters with greater wavelength or intensity, this suppression event is positioned to fall within the HHG ionisation window. Upon increasing the driving wavelength to 1.4 m, the amplitude of the HHG spectrum throughout the high-energy plateau both becomes modulated and includes peaks at non-odd harmonic values. These features coincide with a triple-peak structure in the localisation distribution per half-cycle throughout the central cycles of the laser field in Figure 2(e). The origin of the HHG structures is thus related to the increased nonadiabatic character of the electronic intramolecular motion.

A demonstration of the analysis used to determine whether localisation occurs favourably to modulate the HHG spectrum is shown in Figure 3. By increasing the intensity of the light used in Figure 2(f) to 1.8 × 10^{14} W cm^{-2} and leaving other laser parameters the same, we can produce two instants of ionisation suppression within the HHG ionisation window. This is shown by the two zeroes of the phase difference α (lower panel, [10]). These instants of ionisation suppression are connected to emission of HHG signal at the time of recombination by approximating the electron as a classical point particle, and determining its trajectory analytically [10,12]. This analysis does admit some ambiguity regarding the best approximation for the ionisation and recombination positions. In Figure 3, the extent to which the analysis depends on the selection of these boundary conditions is considered: the dotted line on the left in each set of three lines corresponds to ionisation from $z = 3.5$ and recombination to $z = -3.5$, corresponding to the positions of the nuclear centres; the dotted line in the middle assumes $z = 0$ for both ionisation and recombination; and the dotted line on the right admits the opposite of the first , assuming $z = -3.5$ at ionisation and $z = 3.5$ at recombination. The variance between these conditions is seen to be sufficiently small to preserve a connection between ionisation dynamics and the intervals of HHG suppression. Especially in the case of high-energy features, the large excursion distance travelled by the classical electron reduces the difference between ionisation timings in the three cases to a nearly negligible variance. Use of this classical procedure reliably approximates the timing of HHG suppression, and accurately predicts the number of minima expected per recombination event.

3.2. Generation of radiation at non-integer harmonic frequencies

In addition to a modulated amplitude of radiation emission, HHG signals generated by an electron demonstrating nonadiabatic behaviour can also exhibit a modified structure in the spectral plateau. This modification consists of radiation emission at non-integer harmonic frequencies (c.f., Figure 2(f)). To demonstrate why this structure occurs, we show harmonic signals resulting from sets of three sequential recombination events in Figure 4. In Figure 4(a), these three recombination events are selected from the middle cycles of the driving laser field (9.5–11.25 field cycles). The laser parameters are the same as those used in Figure 2(e,f). Recombination events from this time window are seen

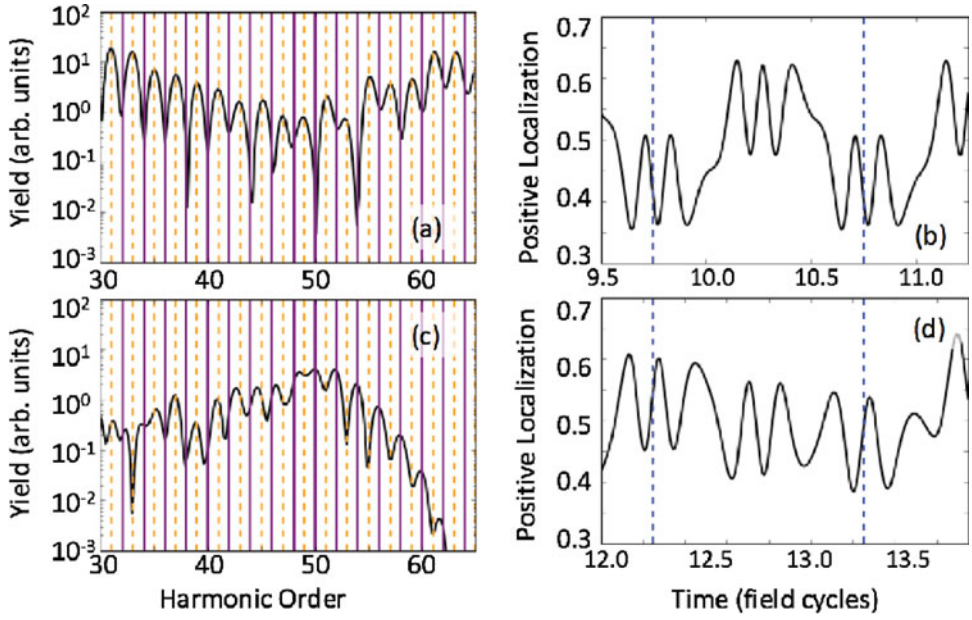

Figure 4. Different sets of recombination events demonstrate a changing interference structure of the HHG. In (a), recombination events occurring near the centre of the driving laser (9.5–11.25 field cycles) result exclusively in odd harmonic generation. Throughout this interval of time, shown in (b), the electron dynamics remain periodic: the same behaviour is observed at each dashed line. In contrast, recombination events considered between 12.0 and 13.75 field cycles (c) exhibit peaks at non-integer or even harmonics. In (d), this is seen to correspond to a changing and aperiodic nonadiabatic dynamics. Both spectra result from driving with a 1.4 m, 20-cycle, 6×10^{13} W cm^{-2} laser field. The position of odd (even) harmonics along the *x*-axis is indicated by dashed (solid) lines.

to interfere to produce exclusively odd harmonics. In contrast, Figure 4(c) shows harmonic generation emitted during a later temporal window, spanning the same number of recombination events (12.0–13.75 field cycles). The HHG produced in this interval shows a transition from odd harmonics emitted at low energies to non-odd harmonics generated at the highest plateau energies.

The generation of odd harmonics is indicative of periodic behaviour in the electron dynamics, which we observe in Figure 4(b). In this time window, the electron dynamics are highly nonadiabatic and we observe several localisations per half-cycle of the driving field. This nonadiabaticity is, however, a periodic behaviour which repeats itself every cycle of the driving field. For example, at each dashed line in Figure 4(b), marking one full laser cycle, we observe the same electron behaviour. So long as the electron dynamics remain the same from one cycle to the next, the intrinsic phase acquired due to these nonadiabatic dynamics will be equivalent at each cycle. Consequently, odd harmonics are generated through the usual HHG mechanism.

This periodicity, observed in Figure 4(b), is induced by the nearly constant laser field amplitude throughout this time interval. As we demonstrated in Equation (3), the timing of localisations is sensitive to the strength of the applied electric field. Consequently, we can destroy the periodicity of the nonadiabatic electron dynamics by modifying the strength of the electric field. This occurs naturally when we use a pulsed laser during the rising and trailing parts of the field. We capture the electron dynamics as the electric field decreases in Figure 4(d). As expected, these dynamics are no longer periodic; the behaviour the electron from one dashed line to the next varies substantially, which results in the non-integer harmonics observed in Figure 4(c). Thus, the interference structure of the emitted radiation will depend sensitively upon changes in the nonadiabatic electron dynamics.

It is additionally notable that the non-odd harmonic generation in Figure 4(c) occurs with equal efficiency to the signal generated during the centre cycles of the laser field, in Figure 4(a). While the interval shown in Figure 4(a) would ordinarily dominate the total signal due to the higher rate of ionisation induced by the stronger electric field, the suppression of harmonic generation due to the transient localisation of the electron on the non-ionising side of the molecular ion reduces the efficiency of harmonic production. The matching amplitudes of harmonic production near the 50th harmonic order in Figure 4(a,c) result in the highly structured interference structure from this portion of the harmonic signal in Figure 2(f); likewise, the absence of ionisation suppression in the HHG signal from Figure 2(d) covers up this effect.

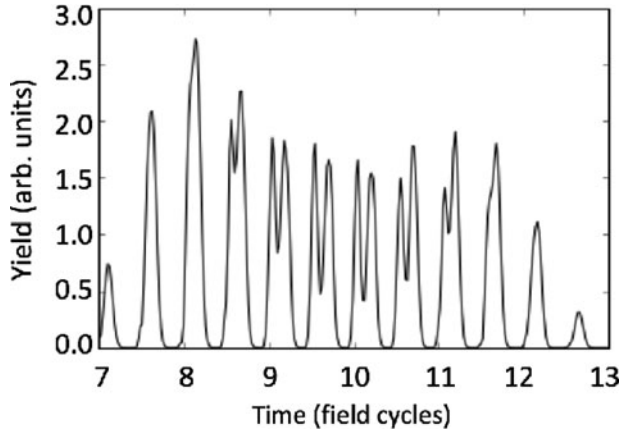

Figure 5. (Colour online) The onset of nonadiabaticity modulates the structure of the attosecond pulses generated. For the same laser field parameters as shown in Figure 1, individual pulses are reduced in amplitude and acquire a double-peak structure near the centre of the field. These features follow from the same mechanism inducing a minimum in the HHG spectrum.

3.3. Attosecond pulse train

As shown above, the effects of transient localisation upon the structure of the HHG spectrum are profound, modifying both the amplitude and interference structure of the plateau if a suitable selection of driving field wavelength and intensity is made. It is natural to question what form these structural changes take when the emitted radiation is considered instead in the time domain of the process. Physically, this time-domain information represents the intensity profile of the emitted radiation pulse, which is considered in the following for an H_2^+ ion driven by 1.8 m light with intensity 6×10^{13} Wcm^{-2}.

The effect of nonadiabaticity upon the generation of attosecond pulses is also pronounced, as demonstrated in Figure 5. In this figure, we transform the energy region spanning 80–120 harmonic orders, capturing the spectral minimum and the extent of the spectrum efficiently producing non-odd harmonics. Throughout the central cycles of the driving laser field, when the nonadiabatic character of the intramolecular electron dynamic is strongest, the reconstructed attosecond pulse train shows deep amplitude modulations. These modulations arise from the same HHG suppression mechanism shown in Figure 3. In the wavelet analysis (Figure 3(a)), we observe a time- and frequency-dependent suppression of HHG emission in the recombination event. The frequency-dependence of this event is the cause of the HHG spectral amplitude modulation seen in Figure 1 to occur at the same energies transformed to create the attosecond pulse train in Figure 5. The corresponding time-dependence is imprinted directly upon the pulse train as the modulation leading to the double-peak structure. The overall width of each pulse is, however, unchanged due to the modification of interference structure and the intrinsic chirp of the harmonic generation process. Consequently, nonadiabatic dynamics can also be seen to modify the structure of attosecond pulses emitted from systems undergoing transient localisation.

4. Phase-matching effects in HHG

Having established the capacity for transient electron localisation to significantly modify both the structure and amplitude of the generated harmonic spectrum, it remains to consider the extent to which these features will remain detectable. In particular, a realistic experimental scenario for the detection of HHG introduces molecular ions at a range of internuclear distances to different effective intensities due to the transverse and longitudinal spatial intensity distributions of the driving laser. Previously, we have shown that the transient localisation signature of a minimum in the HHG spectrum remains present when considering integration of the signal over a range of intensities and internuclear distances [10].

For a HHG signal to be detected, it is also important to consider phase-matching effects to ensure that harmonics emitted at the same energy from different locations in the laser focal region do not interfere destructively. This requirement establishes a criterion for phase-matching that has been productively explored toward the generation of isolated attosecond pulses [20,21]. In the context of detecting nonadiabatic dynamics, the question of phase-matching is particularly relevant due to the modified interference structure of the plateau harmonic energies evident in, for instance, Figure 2(f). In the following, we seek to establish how the modified interference structure additionally alters the phase-matching conditions of the emitted radiation.

Full theoretical analysis of HHG phase-matching would require that we combine the present solutions of the TDSE at the microscopic molecular level with the solution of the Maxwell equations to obtain the macroscopic response. At the long wavelengths needed to induce nonadiabatic dynamics, such an approach is computationally impractical. Instead, we pursue an approximative method to analyse the phase-matching properties of the HHG signal. We assume that a Gaussian beam is used to drive a gas jet sample and seek to estimate both the transverse and longitudinal coherence lengths of radiation emitted by the samples. This is evaluated through the phase mismatch accumulated as $L_{coh}^{\parallel} = \pi/\Delta k_{\parallel}$ and $L_{coh}^{\perp} = \pi/\Delta k_{\perp}$. The respective phase mismatches of any harmonic order q can be calculated as (e.g. [22])

$$\Delta k_q^{\parallel} \approx (q-1)\frac{\partial \zeta(z)}{\partial z} + \frac{\partial \phi_q}{\partial I}\frac{\partial I}{\partial z}, \tag{5}$$

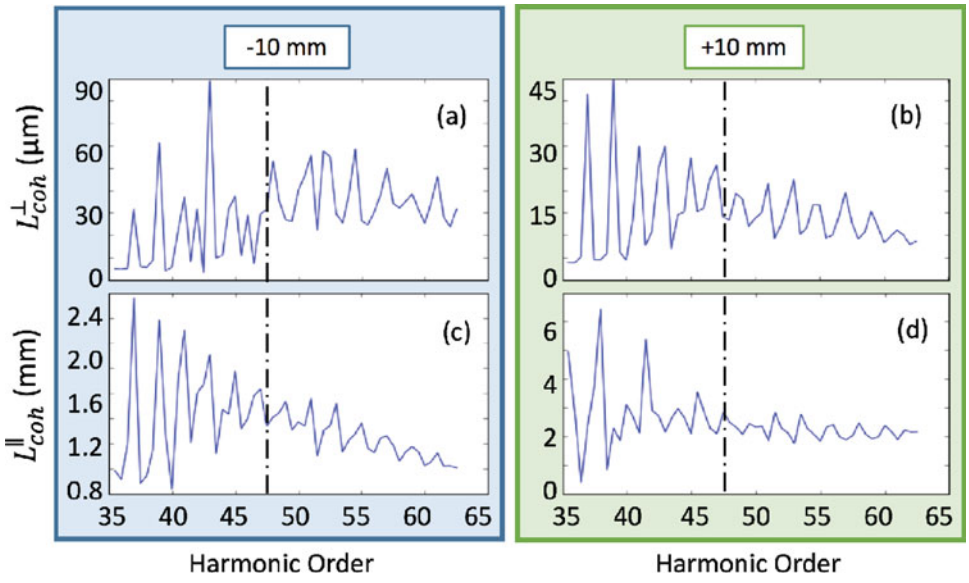

Figure 6. (Colour online) The transverse (a, b) and longitudinal (c, d) coherence lengths of the high-energy HHG plateau indicate qualitative differences between variation and magnitudes of coherences induced by transient electron localisation. In (a) and (c), the gas jet is positioned 10 mm preceding the laser focus; in (b) and (d), the gas jet is set 10 mm after the focus. The driving laser is assumed a Gaussian beam with waist $W_0 = 100$m, peak intensity 7.0×10^{13} Wcm^{-2}, and wavelength 1.4 m. The dashed lines mark the position in the HHG spectrum of the transition from pronounced odd harmonic generation to a more complex interference structure.

where $\zeta(z)$ is the Gouy phase and ϕ_q is the phase of the emitted harmonic of interest, and the density of the gas has assumed to be low enough so that dephasing due to the presence of free charges and neutrals in the sample can be neglected. The intensity of the field is represented by $I(z, \rho)$. In the transverse direction,

$$\Delta k_q^{\perp} \approx -q\frac{\omega}{c}n(\omega)\frac{\rho}{R(z)} + \frac{\partial\phi_q}{\partial I}\frac{\partial I}{\partial\rho}, \tag{6}$$

where $n(\omega)$ is the index of refraction of the sample and $R(z)$ is the radius of curvature of the Gaussian beam.

Within these representations of the phase mismatch, the influence of the nonadiabatic electron dynamic is expressed in the quantity ϕ_q, as all other terms result from the beam properties and the index of refraction of the sample. To estimate $\partial\phi_q/\partial I$, we calculate discrete harmonic spectra at separate fixed peak intensities spanning 5.0×10^{13} to 7.0×10^{13} W cm^{-2} with $\Delta I = 2 \times 10^{12}$ W cm^{-2}. We select the lower bound of these intensities (5.0×10^{13} W cm^{-2}) by acknowledging that HHG spectra emitted by weaker driving fields will result plateau energy emission with decreasing efficiency. These weak HHG spectra are assumed to contribute negligibly to the total HHG signal emitted by the Gaussian beam. At 5.0×10^{13} W cm^{-2}, we find that the plateau efficiency is two orders of magnitude less than the minimum plateau amplitude generated at 7.0×10^{13} W cm^{-2}. Consequently, when calculating features such as phase-matching that consider the composite contributions of several distinct driving intensities, we need only calculate contributions within the indicated range. We note that this discrete intensity approximation introduces variation in the coherence lengths predicted by the model. In the following figures, we present the median value of the predicted coherence lengths, which accurately follows the aggregate behaviour of the phase-matching predictions. In calculations of $\Delta k_q^{\perp}$, we estimate that $n(\omega) \approx 1.5$ as a reasonable value for the wavelengths presented, noting that any value spanning $1 \leq n(\omega) \leq 2$ produces the same result in the following analysis.

In Figure 6(a–d), we present the respective transverse and longitudinal phase-matching behaviour of harmonics generated throughout the plateau energies using a driving wavelength of 1.4 m. The Gaussian laser beam is assumed to have peak intensity 7.0×10^{13} W cm^{-2} with a beam waist of $w_0 = 100$ m. In Figure 6(a,c), the placement of the gas jet is modelled at 10 mm preceding the focus; in Figure 6(b,d), the jet is placed 10 mm after the focus. In each case, the dashed line demarcates the boundary between the energy regime in which conventional odd harmonics are emitted and that in which the interference structure becomes more complex.

The two instances of transverse phase-matching demonstrate similar qualitative differences between the two energy regimes. As seen in Figure 6(a), in the low-energy region, odd harmonics maintain coherence over greater distances than any other value. In contrast, the

coherence lengths of photon energies emitted throughout the second regime of the complex HHG interference structure demonstrate greater consistency. Non-odd harmonic values are emitted with equivalent coherence lengths to odd harmonic values, with an average magnitude comparable to that of odd harmonics emitted in the first region. In Figure 6(b), the positioning of the gas jet following the laser focus generally reduces the coherence length of all emitted harmonics. Nevertheless, similar trends are shown: odd harmonic detection is strongly favoured in the first region, while all energy values in the second region are emitted with less variant coherence lengths. In each case, the coherence lengths of radiation emitted at energies signalling nonadiabatic electron dynamics are sufficiently long to permit detection.

The longitudinal phase-matching is examined in Figure 6(c,d). In this case, positioning the gas jet prior to the focus is seen to reduce the coherence lengths of emitted photons in comparison with placement after the focus. In Figure 6(d), similar behaviour to transverse phase-matching is clearly observed: all values throughout the highest energy section of the plateau demonstrate similar efficiency as the odd harmonics in the first section with greater magnitude than the preceding non-odd harmonics. The pre-focus gas jet positioning of Figure 6(c) ultimately reduces the coherence lengths of the highest energy values due to the dominance of the Gouy phase term in determining the magnitude of the phase mismatch. However, comparison of proximal energy intervals exhibiting difference interference behaviours in the HHG spectrum show similar features described in the analysis of Figure 6(d). In each case, the coherence lengths are again sufficient to enable the detection of the transient localisation signatures.

5. Conclusions

In this paper, we have demonstrated the capacity for transient electron localisation to strongly modify and modulate HHG. We have studied this behaviour in the context of a fixed internuclear distance model for H_2^+, for which the nonadiabatic behaviour of interest is well understood. In addition to developing our understanding for the conditions which enable transient electron localisation to suppress harmonic emission at critical energy intervals, we have also explored the mechanism causing the highly structured interference pattern at the highest plateau energies of molecules undergoing nonadiabatic electron behaviour. Breaking the inversion symmetry of the electron distribution at the time of recombination during sequential half-cycles of the laser field is seen to produce non-odd harmonics. Producing this modified interference structure within the total HHG spectrum relies upon the modulation of the HHG signal, which equalises the amplitude of harmonic emission during the middle field cycles and along the rising and trailing ends of the field. Additionally, transient electron localisation is seen to modify the time-domain structure of the emitted radiation through the same mechanism that modulates the HHG amplitude. Individual peaks within the yielded pulse train are seen to acquire a two-peak feature due to intervals of suppressed emission during electron wavepacket recombination. In addition to efficiently yielding non-odd harmonics, transient electron localisation alters the accumulated phase mismatch of radiation throughout the highest energies of the HHG plateau. Non-odd harmonic energy values acquire coherence lengths of comparable value to odd harmonic values in this regime along both the transverse and longitudinal planes of the modelled Gaussian beam. This property assists the detection of the HHG signal in this regime. In total, these findings show that HHG is a sensitive tool for the detection of nonadiabatic intramolecular electron dynamics. Both the amplitude and phase of each harmonic encode events ongoing during ionisation and recombination of the electron wavepacket. In turn, the capacity for nonadiabatic electron dynamics to strongly modify the spectral content of the emitted radiation offers a potential method for further customising attosecond pulses and for imaging the laser-driven behaviour of electrons inside of molecules.

Acknowledgments

The authors acknowledge Carlos Hernandez-Garcia for discussions.

Disclosure statement

No potential conflict of interest was reported by the authors.

Funding

M. R. Miller was supported by the National Science Foundation Graduate Research Fellowship [grant number DGE 1144083], the US Department of Energy Office of Basic Energy Science, Chemical Sciences, Geosciences and Biosciences Division, Atomic, Molecular and Optical Sciences Program [award number DE-FG02-09ER16103] and the US National Science Foundation [grant number PHY-1125844]. A. Jaroń-Becker was supported by the US National Science Foundation [grant number PHY-1125844] and the Air Force Office of Scientific Research [award number FA9550-16-1-0121]. A. Becker was supported by the US Department of Energy Office of Basic Energy Science, Chemical Sciences, Geosciences and Biosciences Division, Atomic, Molecular and Optical Sciences Program [award number DE-FG02-09ER16103]. This work utilised the Janus supercomputer, which is supported by the US National Science Foundation grant number CNS-0821794 and operated by the University of Colorado Boulder.

References

[1] M.R. Miller, Y. Xia, A. Becker, and A. Jaron-Becker, Optica **3**, 259 (2016).
[2] M. Lezius, V. Blanchet, D.M. Rayner, D.M. Villeneuve, A. Stolow, and M.Y. Ivanov, Phys. Rev. Lett. **86**, 51 (2001).
[3] M. Lezius, V. Blanchet, M.Y. Ivanov, and A. Stolow, J. Chem. Phys. **117**, 1575 (2002).
[4] F. He, A. Becker, and U. Thumm, Phys. Rev. Lett. **101**, 213002 (2008).
[5] M. Odenweller, N. Takemoto, A. Vredenborg, K. Cole, K. Pahl, J. Titze, L.Ph.H. Schmidt, T. Jahnke, R. Dörner, and A. Becker, Phys. Rev. Lett. **107**, 143004 (2011).
[6] P.-L. He, N. Takemoto, and F. He, Phys. Rev. A, **91**, 063413 (2015).
[7] I. Bocharova, R. Karimi, E.F. Penka, J.-P. Brichta, P. Lassonde, X. Fu, J.-C. Kieffer, A.D. Bandrauk, I. Litvinyuk, J. Sanderson, and F. Legare, Phys. Rev. Lett. **107**, 063201 (2011).
[8] T. Zuo and A.D. Bandrauk, Phys. Rev. A. **52**, R2511 (1995).
[9] T. Seideman, M.Y. Ivanov, and P.B. Corkum, Phys. Rev. Lett. **75**, 2819 (1995).
[10] M.R. Miller, A. Jaroń-Becker, and A. Becker, Phys. Rev. A. **93**, 013406 (2016).
[11] Y. Xia and A. Jaron-Becker, Opt. Express. **24**, 4689 (2016).
[12] P.B. Corkum, Phys. Rev. Lett. **71**, 1994 (1993).
[13] K.J. Schafer, B. Yang, L.F. DiMauro, and K.C. Kulander, Phys. Rev. Lett. **70**, 1599 (1993).
[14] J. Itatani, J. Levesque, D. Zeidler, H. Niikura, H. Pepin, J.C. Kieffer, P.B. Corkum, and D.M. Villeneuve, Nature **432**, 867 (2004).
[15] M. Lein, N. Hay, R. Velotta, J.P. Marangos, and P.L. Knight, Phys. Rev. Lett. **88**, 183903 (2002).
[16] N. Takemoto and A. Becker, Phys. Rev. Lett. **105**, 203004 (2010).
[17] N. Takemoto and A. Becker, Phys. Rev. A **84**, 023401 (2011).
[18] S. Chelkowski, A. Conjusteau, T. Zuo, and A. Bandrauk, Phys. Rev. A. **54**, 3235 (1996).
[19] N. Takemoto and A. Becker, J. Chem. Phys. **134**, 074309 (2011).
[20] T. Popmintchev, M.-C. Chen, P. Arpin, M.M. Murnane, and H.C. Kapteyn, Nat. Photon. **4**, 822 (2010) .
[21] T. Popmintchev, M.-C. Chen, D. Popmintchev, P. Arpin, S. Brown, S. Ališauskas, G. Andriukaitis, Tadas Balčiunas, O.D. Mücke, A. Pugzlys, A. Baltuška, B. Shim, S.E. Schrauth, A. Gaeta, C. Hernández-García, L. Plaja, A. Becker, A. Jaron-Becker, M.M. Murnane, and H.C. Kapteyn, Sci. **336**, 1287 (2012).
[22] C. Hernandez-Garcia, I.J. Sola, and L. Plaja, Phys. Rev. A **88**, 043848 (2013).